PAPER • OPEN ACCESS

Evaluation of single-sided nuclear magnetic resonance technology for usage in geosciences

To cite this article: Stephan Costabel *et al* 2023 *Meas. Sci. Technol.* **34** 015112

View the article online for updates and enhancements.

You may also like

- SiS Formation in the Interstellar Medium through Si+SH Gas-phase Reactions
V. C. Mota, A. J. C. Varandas, E. Mendoza et al.
- Crystal structure and photoluminescence of $(Gd,Ce)_4(SiS_4)_3$ and $(Y,Ce)_4(SiS_4)_3$
Yasushi Nanai, Katsuhiro Suzuki and Tsuyoshi Okuno
- Strain-dependent optical properties of the novel monolayer group-IV dichalcogenides SiS_2 semiconductor: a first-principles study
Qing-Yuan Chen, Ming-Yang Liu, Chao Cao et al.

Breath Biopsy® OMNI®
The most advanced, complete solution for global breath biomarker analysis

TRANSFORM YOUR RESEARCH WORKFLOW


Expert Study Design & Management


Robust Breath Collection

Reliable Sample Processing & Analysis


In-depth Data Analysis


Specialist Data Interpretation

This content was downloaded from IP address 194.95.157.29 on 09/02/2023 at 12:37

OPEN ACCESS
IOP Publishing
Measurement Science and Technology
Meas. Sci. Technol. **34** (2023) 015112 (13pp)
https://doi.org/10.1088/1361-6501/ac9800

Evaluation of single-sided nuclear magnetic resonance technology for usage in geosciences

Stephan Costabel[1,*], Thomas Hiller[1,5], Raphael Dlugosch[2,6], Sabine Kruschwitz[3] and Mike Müller-Petke[4]

[1] Federal Institute for Geosciences and Natural Resources, Berlin, Germany
[2] Federal Institute for Geosciences and Natural Resources, Hanover, Germany
[3] Bundesanstalt für Materialforschung und -prüfung, Berlin, Germany
[4] Leibniz Institute for Applied Geophysics, Hanover, Germany

E-mail: stephan.costabel@bgr.de

Received 4 May 2022, revised 29 September 2022
Accepted for publication 6 October 2022
Published 21 October 2022

Abstract

Because of its mobility and ability to investigate exposed surfaces, single-sided (SiS) nuclear magnetic resonance (NMR) technology enables new application fields in geosciences. To test and assess its corresponding potential, we compare longitudinal (T_1) and transverse (T_2) data measured by SiS NMR with those of conventional geoscientific laboratory NMR. We use reference sandstone samples covering a broad range of pore sizes. Our study demonstrates that the lower signal-to-noise ratio of SiS NMR data generally tends to slightly overestimated widths of relaxation time distributions and consequently pore size distributions. While SiS and conventional NMR produce very similar T_1 relaxation data, unbiased SiS NMR results for T_2 measurements can only be expected for fine material, i.e. clayey or silty sediments and soils with main relaxation times below 0.05 s. This limit is given by the diffusion relaxation rate due to the gradient in the primary magnetic field associated with the SiS NMR. Above that limit, i.e. for coarse material, the relaxation data is strongly attenuated. If considering the diffusion relaxation time of 0.2 s in the numerical data inversion process, the information content >0.2 s is blurred over a range larger than that of conventional NMR. However, our results show that principle range and magnitudes of the relaxation time distributions are reconstructed to some extent. Regarding these findings, SiS NMR can be helpful to solve geoscientific issues, e.g. to assess the hydro-mechanical properties of the walls of underground facilities or to provide local soil moisture data sets for calibrating indirect remote techniques on the regional scale. The greatest opportunity provided by the SiS NMR technology is the acquisition of profile relaxation data for rocks with significant bedding structures at the µm scale. With this unique feature, SiS NMR can support the understanding and modeling of hydraulic and diffusional anisotropy behavior of sedimentary rocks.

[5] Formerly: Rheinisch-Westfälische Technische Hochschule (RWTH) Aachen, Germany.
[6] Formerly: Leibniz Institute for Applied Geophysics, Hanover, Germany.
[*] Author to whom any correspondence should be addressed.

Original Content from this work may be used under the terms of the Creative Commons Attribution 4.0 licence. Any further distribution of this work must maintain attribution to the author(s) and the title of the work, journal citation and DOI.

 © 2022 The Author(s). Published by IOP Publishing Ltd

Keywords: geosciences, nuclear magnetic resonance, single-sided NMR

(Some figures may appear in colour only in the online journal)

1. Introduction

Applications for measuring nuclear magnetic resonance (NMR) are well established in geophysics. In the laboratory, in boreholes, or from the Earth's surface, they provide relevant information on porous geo-materials, e.g. type and content of the pore liquid, porosity, diffusivity, pore size distribution, permeability, etc. In doing so, ^{1}H nuclei as molecular component of water and hydrocarbon are the usual objectives of investigation. Their proton spins cause a magnetic moment, which is aligned with an external static magnetic field. Correspondingly, a ^{1}H spin ensemble, e.g. a sample consisting of water or oil, exhibits a spin magnetization with the same orientation as the static (primary) magnetic field.

NMR devices manipulate this spin magnetization by electromagnetic pulses, i.e. alternating magnetic fields matching the resonance frequency of the spin system, the Larmor frequency (Levitt 2002). They stimulate and subsequently detect a response signal corresponding to the relaxation process of the spin system, which returns to its equilibrium state in the primary magnetic field. The signal strength is linear to the amount of stimulated ^{1}H nuclei in the observed volume, so water and/or hydrocarbon content can be estimated (Flaum *et al* 1998, Behroozmand *et al* 2014, Müller-Petke and Yaramanci 2015). The relaxation behavior of the NMR signal encodes structural and mineralogical information of the pore surface and allows the analysis of, for instance, pore size distribution and permeability (Kenyon 1997, Dlugosch *et al* 2013, Knight *et al* 2015), the level of pore surface fractality (Pape *et al* 2006, Zhang and Weller 2014, Müller-Petke *et al* 2015), or the quality of iron-oxide coating on the pore walls (Keating and Knight 2007, Costabel *et al* 2018). Specialized pulsing techniques combined with specific experimental setups provide estimates of diffusion coefficients in the porous material under investigation (Seland *et al* 2004, Kolz *et al* 2007) and characterize the mobility of water molecules through the pore space (Romanenko *et al* 2012, Hiller *et al* 2020).

NMR in geophysical applications is available for different investigation scales. Samples and drilling cores with sizes of a few cubic centimeters to cubic decimeters are investigated with laboratory NMR (Keating and Knight 2007, Romanenko *et al* 2012, Zhang and Weller 2014, Hiller *et al* 2020), where they are placed inside a measurement coil system embedded in a strong homogeneous magnetic field. Coils and magnets are arranged and adjusted in a way to control and optimize the corresponding excitation fields for a very precise manipulation and exact registration of the involved spin dynamics. Compared to such laboratory equipment, NMR measurements conducted in boreholes are limited in precision. Corresponding tools exhibit sizes from 1 to 10 m for groundwater and hydrocarbon characterization, respectively, and include a permanent magnet generating a magnetic field on the outside of the probe. Consequently, this field is inhomogeneous in the investigated formation and decreases with increasing distance from the borehole. The measurement coil system of such borehole equipment can produce a relevant spin excitation only within a small volume around the probe having the shape of a thin shell (Kleinberg *et al* 1992, Walsh *et al* 2013). The measurement signal is correspondingly small and the excitation inside the gradient field cannot be realized without certain off-resonance components. The same is also true for the application of the so-called surface NMR method, where large cable loops on the Earth's surface are utilized for groundwater exploration and aquifer characterization (Vouillamoz *et al* 2012, Behroozmand *et al* 2014, Lesparre *et al* 2020). These methods use the Earth's magnetic field as primary field and produce measurable signals only by exciting large volumes in the subsurface.

Blümich *et al* (2008) demonstrated a novel type of NMR measurement equipment, the so-called single-sided (SiS) NMR technique, which is in a sense a small-scaled mixture of the borehole and surface NMR technologies. The most relevant property of SiS NMR is its mobility. Corresponding devices are small and thus easy to handle for directly and non-invasively investigating the moisture of exposed surfaces. Consequently, this technology is applied in quality control, food, and material sciences, e.g. for identifying imperfections or hidden failures in textiles (Kolz *et al* 2007, Blümich *et al* 2008), testing the condition of meat (Blümich *et al* 2008), or monitoring the interaction of water and building material (Schulte Holthausen and Raupach 2018). With a sensitive measurement volume formed as a thin slice on a footprint in the cm^2 range, it also opens new fields of geophysical applications:

(a) Investigation of samples directly after taking them, i.e. without risking alteration on the way to the laboratory such as evaporation or oxidation (figure 1(a)).
(b) In-situ measurements on walls of underground facilities (figure 1(b)) to test and control their moisture state. Such investigations contribute to the assessment of stability and integrity of tunnels, mines, and underground repositories (Ziefle *et al* 2017).
(c) In-situ soil measurements in the first few mm to cm (figure 1(c)) to acquire valuable calibration and controlling data sets for regional remote measurement techniques (Koch *et al* 2021).
(d) Hydraulic characterization of bedding structures of sedimentary rocks in the µm to mm range that often control their anisotropic hydraulic properties on much larger scales (Sato *et al* 2019).

The mobility option of SiS devices comes at the cost of a NMR measurement inside a strong magnetic gradient field, similar to, but much stronger than those in borehole tools. As

Figure 1. Potential application fields for single-sided (SiS) NMR in geosciences: (a) mobile NMR for investigating samples immediately after taking them, i.e. an analysis without the risk of chemical altering or evaporation, (b) in-situ moisture measurements on tunnel walls, e.g. a relevant contribution to the stability and integrity assessment of underground facilities, (c) non-invasive soil moisture measurements.

shown in detail in the following section, this SiS NMR gradient field leads to an additional relaxation component, the so called diffusion relaxation, that might dominate the relaxation process and thus blurs the desired information of the investigated pore structure. To the best of our knowledge, systematic studies aiming on this issue have not been conducted to date. It seems that a detailed quantitative analysis of the SiS NMR relaxation behavior compared to conventional NMR applications has not been required, because the use of the SiS NMR technology in the application fields mentioned above is either focused solely on the signal amplitude (which is related to the amount of water in the material) or on relative changes of the relaxation process.

In this study, we investigate a set of 18 different natural sandstones, which cover a broad range of pore sizes, using SiS NMR relaxation and compare the corresponding results with conventional laboratory NMR. In doing so, we produce reference data sets of longitudinal (T_1) and transverse (T_2) relaxation time distributions (RTDs) and identify the conditions, under which the SiS technology provides correct RTDs. We consider the influence of the diffusion relaxation in the usual multi-exponential data approximation and analyze its performance to reconstruct the RTD by determining a set of relevant statistical quantities. Finally, we discuss and assess the potential use of SiS NMR within the scope of the identified geophysical application fields mentioned above.

2. Theoretical background

2.1. General NMR

When stimulating the NMR of a ^{1}H spin ensemble, two relaxation mechanisms can be observed:

- the longitudinal (T_1) relaxation, which is observed parallel to the primary magnetic field $\mathbf{B}_0$.
- the transverse (T_2) relaxation, which is observed in the plane perpendicular to $\mathbf{B}_0$.

These mechanisms behave characteristically different in porous media and have their individual advantages and disadvantages in the context of geophysical applications. For details on the NMR phenomenon in general and measurement principles of NMR relaxometry, we refer to Levitt (2002) and other textbooks. Specific information on geophysical NMR applications can be found for instance in Coates *et al* (1999) and Dunn *et al* (2002). Here, we are interested only in the differences of the underlying relaxation components related to the measurement environment of the SiS NMR technology.

In case of T_1 relaxation in a water-filled porous medium, the measured response signal E as a function of time t is described by a multi-exponential behavior:

$$\frac{E(t)}{E_0} = 1 - \sum_i I_i \exp\left(-\frac{t}{T_{1,i}}\right) = 1 - \sum_i I_i \exp\left(-\frac{t}{T_{1\mathrm{S},i}} - \frac{t}{T_{1\mathrm{B}}}\right), \quad (1)$$

where E_0 is the signal amplitude at $t = 0$, I_i is the relative intensity of the relaxation regime corresponding to the individual relaxation rates $1/T_{1,i}$ (and $1/T_{1\mathrm{S},i}$), and $1/T_{1\mathrm{B}}$ is the bulk relaxation rate. The subscript 'S' refers to 'surface relaxation' and indicates that the i-th relaxation regime is usually associated with a specific surface-to-volume ratio, i.e. with a specific pore size. $T_{1\mathrm{B}}$ is the relaxation time of the bulk pore fluid, which is often much longer than $T_{1\mathrm{S},i}$ and therefore negligible.

The resonance frequency of the proton spin increases linearly with increasing $\mathbf{B}_0$ strength (Levitt 2002). Thus, stimulated spins with slightly different resonance frequencies (due to unavoidable inhomogeneities of $\mathbf{B}_0$) loose their coherence when observed perpendicular to $\mathbf{B}_0$. For exact T_2 measurements, this effect has to be corrected by specific rephasing pulses (the Carr-Purcell-Meiboom-Gill, CPMG, pulse sequence, (Carr and Purcell 1954, Meiboom and Gill 1958)). For a perfect rephasing, the resonance frequency of the single spins in the ensemble must not change during the experiment. However, if the level of the $\mathbf{B}_0$ inhomogeneity is high enough, which is the case in SiS NMR, the spins change their frequencies by diffusing through regions with different $\mathbf{B}_0$ strengths. The consequence is an imperfect rephasing and the relaxation process is enhanced due to the corresponding loss of coherence between the spins. Hence, the T_2 response signal exhibits an additional exponential relaxation rate compared to T_1, the

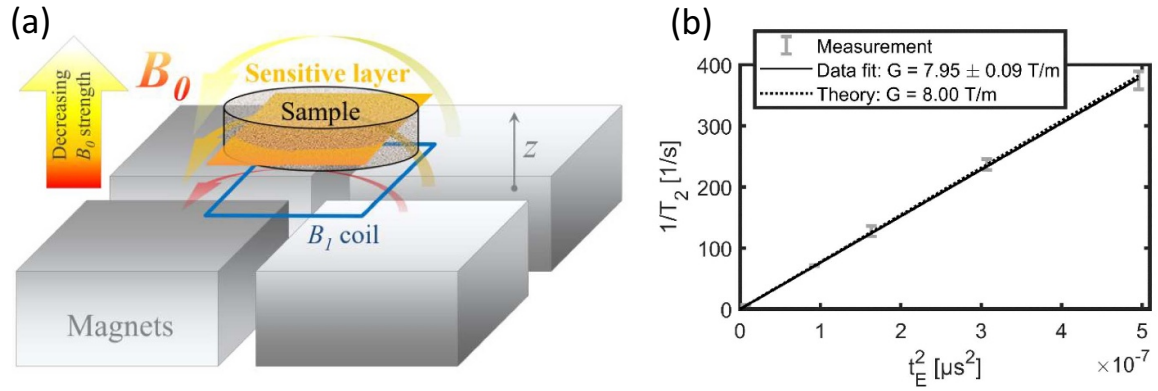

Figure 2. (a) Schematic of magnet and coil arrangement and resulting sensitivity volume of the single-sided (SiS) NMR device (Blümich *et al* 2008), (b) transverse relaxation rate ($1/T_2$) as function of the squared echo time (t_E^2) for a water sample to visualize the influence the corresponding diffusion relaxation inside the $\mathbf{B}_0$ gradient field.

diffusion relaxation rate $1/T_{2D}$ (Coates *et al* 1999, Dunn *et al* 2002, Levitt 2002, Keating and Knight 2007):

$$\frac{E(t)}{E_0} = \sum_i I_i \exp\left(-\frac{t}{T_{2,i}}\right) = \sum_i I_i \exp\left(-\frac{t}{T_{2S,i}} - \frac{t}{T_{2D}} - \frac{t}{T_{2B}}\right), \quad (2)$$

where $T_{2S,i}$ and T_{2B} are defined according to the corresponding T_1 components above and carry, in principle, the same information content. Assuming a linear gradient G, the diffusion relaxation is computed by (Kleinberg and Horsfield 1990)

$$\frac{1}{T_{2D}} = \frac{D(\gamma G t_E)^2}{12}, \quad (3)$$

with the diffusion coefficient D (=2.025×10^{-9} m^2 s^{-1} at 20 °C), the gyromagnetic ratio of the hydrogen proton γ (=0.267×10^9 rad(Ts)$^{-1}$), and the echo time t_E. The latter is an adjustable measurement parameter that controls the time between subsequent rephasing pulses.

It is noteworthy that the T_2 data acquisition can be realized much faster than T_1 and commonly provides time series with higher sampling frequencies. This is the reason why many geophysical applications use T_2 and accept the possible distortion by T_{2D}.

2.2. Single-sided NMR

As mentioned above, the main idea of the SiS NMR technique is to provide the sensitive measurement volume on the outside of the apparatus, which enables non-invasive measurements by getting the device in touch with the investigation object (Blümich *et al* 2008). Figure 2(a) schematically shows the basic structure of a SiS NMR device as used in this study: four single permanent magnets realize a $\mathbf{B}_0$ gradient field that decreases in strength with increasing distance to the magnets. A measurement coil with dimensions in the cm range is arranged as such that a thin sensitive volume is formed, a plane with a thickness of 0.1 mm to 0.2 mm and fixed horizontal dimensions determined by the shape of the loop (40 by 40 mm^2 in this study). Because of the linear relationship between Larmor frequency and $\mathbf{B}_0$ field strength, the exact position of the sensitive footprint is controlled by the operating frequency of the system. The lower the transmitted frequency, the larger is the distance of the sensitive plane from the surface of the magnet.

A T_2 measurement taking place in the gradient field of a SiS NMR apparatus naturally causes a non-negligible $1/T_{2D}$ component (see equation (2)). Its contribution can be discovered by subsequent measurements with varying echo time t_E as depicted in figure 2(b) using a pure water sample. The linear slope of the resulting $1/T_2$ rates, when plotted against t_E^2 and approximated by equation (3), provides the gradient strength inside the sensitive volume. The corresponding result of our measurements in figure 2(b) validates the theoretical value given for the device used in this study.

2.3. Problem statement

For geophysical NMR applications with focus on estimating pore size information, only the surface relaxation rate is important, i.e. the terms $1/T_{1S,i}$ and $1/T_{2S,i}$ in equations (1) and (2), respectively. For simplification, we ignore the index i referring to varying pore size clusters for the following explanations and use the notation $T_{1,2}$ if the corresponding statements are true for both the longitudinal and the transverse relaxation process. When measuring inside the homogeneous $\mathbf{B}_0$ field of conventional laboratory NMR the diffusion relaxation ($1/T_{2D}$) is negligible, unless ferromagnetic minerals inside the pore space generate gradient fields at the pore scale (Keating and Knight 2007, Keating *et al* 2008). Moreover, $1/T_{1,2B}$ is normally much smaller than $1/T_{1,2S}$, which usually allows the assumption that

$$\frac{1}{T_{1,2}} \approx \frac{1}{T_{1,2S}}. \quad (4)$$

Figure 3 depicts T_2 as a function of T_{2S} assuming $T_{2B} = 2.5$ s (dotted line) and demonstrates that the difference between the

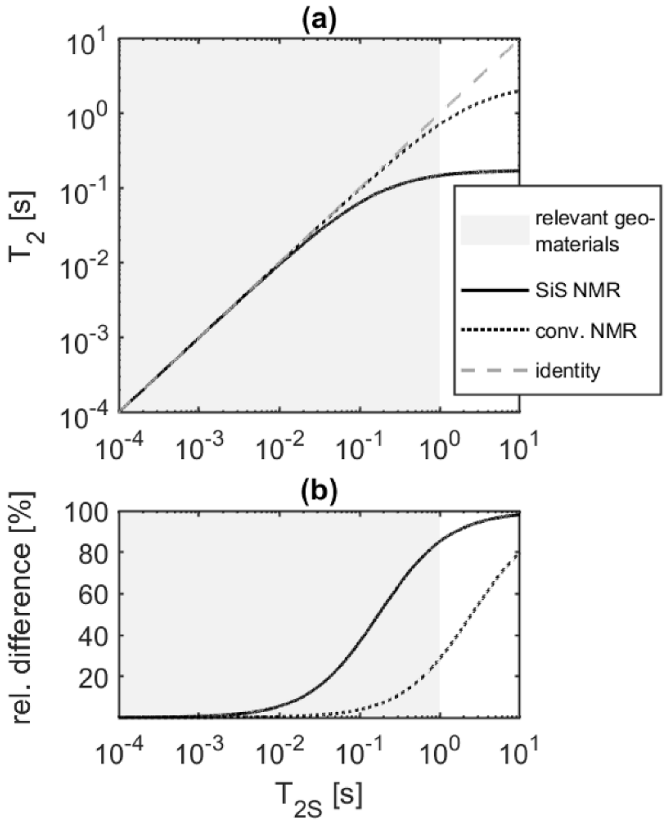

Figure 3. (a) transverse relaxation time T_2 as measured using single-sided (SiS) and conventional NMR as a function of surface relaxation time T_{2S}, (b) relative difference between T_2 and T_{2S}. The calculation of T_2 according to equation (2) considers $T_{2B} = 2.5\,s$ (for both SIS and conv. NMR) and $T_{2D} = 0.2\,s$ (for SiS NMR only). The latter value corresponds to the SiS NMR apparatus used in this study at an echo time of 80 µs.

two is only significant for very long relaxation times at the edge of the range relevant for geo-materials. However, the consequence of T_2 measurements in the gradient field of a SiS NMR device is a non-negligible $1/T_{2D}$ that enhances the relaxation much more than $1/T_{2B}$ as shown in figure 3. The corresponding graph (solid black line) assumes $T_{2D} = 0.2\,s$ in accordance to the properties of the device that we use in this study at an echo time of 80 µs. The T_2 curve in figure 3(a) converges to T_{2D}, meaning that long relaxation components will be compressed to $T_2 < 0.2\,s$. We note from figure 3(b) that the range influenced by the diffusion relaxation already starts at a few ms. However, from the practical viewpoint only the effect on $T_2 > 0.05\,s$ seems to be significant, because at this range the relative difference with more than 30% starts becoming visible at the logarithmic scale, at which NMR relaxation times are usually interpreted in geosciences.

3. Material and methods

3.1. NMR measurements using water-saturated sandstone samples

We investigate a set of 18 sandstone samples with dominating pore sizes ranging from 0.1 to 50 µm, i.e. cylindrical drill cores with diameters of 20.0 and 25.5 mm (table 1). The samples were saturated with de-mineralized water using a vacuum desiccator and afterwards kept in a water bath to maintain their saturated state. After taking them out for conducting the NMR measurements, we carefully removed remaining water drops on their surfaces and covered the samples in plastic foil to prevent them from evaporation during the experiments.

Table 1. List of samples.

Sample name	Specification	Porosity (vol.%)	Dominating pore size (µm)
Mu3	Mucharz	4.5	0.1
San4	Sander	18.5	8.4
Wei4	Weiberner Tuffstein	46.1	3.7
Sch14	Schleeriether	16.3	1.2
R5	Röttbacher	16.6	9.8
Ett4	Ettringer Tuffstein	33.5	2.9
Ob14	Obersulzbacher	20.8	4.1
Gr54	Gravenhorster	14.2	6.7
C1s	Cottaer	21.7	18.3
Gr55	Gravenhorster	14.2	6.7
C1p	Cottaer	21.7	18.3
Lan4	Langenauer	12.0	2.1
Ud11	Udelfanger	23.5	18.3
Ber1	Berea	19.8	14.5
Ska1s	Skala	24.8	29.0
10^{-2}	Elbsandstein	18.5	49.2
Deu1	Deutmannsdorfer	19.3	44.2
S1b	Bentheimer	18.8	22.8

The SiS NMR measurements were carried out with a NMR-Mouse PM25 (Magritek). The conventional NMR measurements used a rock core analyzer based on a Halbach-array setup, which realizes an almost perfect homogeneous static magnetic field inside the sample opening (Halbach 1980, Anferova *et al* 2007). The data are published under an open access license (Costabel *et al* 2022). Essential device specifications and measurement parameters are given and compared in table 2. The T_1 relaxation was measured using the saturation recovery sequence (Levitt 2002) and the T_2 relaxation was measured using the CPMG sequence mentioned above. After performing a rapid tentative measurement using a standard parameter configuration for a specific sample, the parameter configuration for its regular measurement was optimized individually in a way that a trade-off between total measurement time (=time for averaging measurement repetitions) and acceptable noise level was achieved.

In addition to the unavoidable influence of the diffusion relaxation, the signal-to-noise ratio (SNR) of SiS NMR data is generally lower than that of conventional NMR because the measurement volume is orders of magnitudes smaller. Noisier data lead to a higher level of uncertainty for the estimation of the wanted pore parameters, which could only be prevented by increasing the number of measurement repetitions for averaging (stacking). However, regarding a feasible application this is only economic and thus meaningful up to a certain level.

Table 2. List of relevant NMR measurement parameters and device specifications.

Measurement parameter/ specification	Single-sided NMR	NMR rock core scanner
Working frequency	13.1 MHz	3.9 MHz
T_1 recovery times	0.2 to max. 6000 ms	0.5 to max. 7000 ms
Number of T_1 recovery times	70 to 100	85 to 120
Average T_1 noise level[a]	0.35 to 0.6%	0.2 to 0.3%
Mean T_1 measurement time/sample	300 to 400 min	60 to 120 min
T_2 echo time	80 µs	231 µs
Number of echos	200 to 6000	1500 to 16 000
Repetition time	2 to 60 s	2 to 10 s
Average T_2 noise level [a]	1.3 to 4.5%	0.4 to 0.7%
Mean T_2 measurement time/sample	60 to 270 min	10 to 30 min

[a] The relative noise level refers to the root mean square (RMS) value of the data fit divided by the initial amplitude of the signal.

For this reason, we decided to limit the total measurement time for one sample using the SiS NMR to a few hours at maximum. As can be noted from table 2, the resulting times for single T_1 or T_2 measurements using SiS NMR exceed those of the core analyzer many times over. Nevertheless, their resulting relative noise levels are still worse on average.

In contrast to the conventional NMR measurements, where the samples are investigated as a whole, the SiS NMR device observes only a part of it, as mentioned above, a thin slice with a thickness of about 0.2 mm. The apparatus is intended for investigating vertical moisture profiles with a resolution at the sub-millimeter scale inside specimens that are simply placed on a table above the device (Kolz *et al* 2007, Blümich *et al* 2008). For that purpose, the device is mounted on an elevator (Perlo *et al* 2005), which can continuously be moved up and down with a step size of 0.05 mm. Our SiS NMR measurements using the sample cylinders (figure 4) are repeated at five different heights separated by 2.5 mm from one another. To reconstruct to some extent the integrated information of conventional NMR these time series are averaged before the multi-exponential fitting.

However, the opportunity of SiS NMR to provide slice-wise information on the internal small-scaled structure of specific geological material is an interesting feature, i.e. for investigating small-scaled bedding planes of sedimentary rocks and shales (Sato *et al* 2019). As an example to demonstrate the benefit of such experiments, we repeated the T_2 measurements using the Berea sandstone with an increased vertical step size of 0.25 mm. As obvious from the photograph in figure 4 by the alternating strata of grayish and reddish colors, the Berea sandstone is characterized by thin parallel layers in the mm-range. These layers demonstrate the alternating sedimentation

Figure 4. Berea sandstone sample on the SiS NMR sensor. The photograph was arranged to make the stratification of the rock visible. During the regular measurements of this study, the samples were covered in plastic foil to prevent evaporation during the NMR experiments.

conditions, under which this kind of rock was formed. Quartz sand particles in the planes with reddish color are mixed with opaque mineral grains (Sato *et al* 2019), whereas these impurities are absent in those areas with gray color. Sato *et al* (2019) demonstrate that the mineral mixture in the bedding planes of Berea sandstones has a significant impact on the pore water mobility and causes a high level of anisotropy of permeability, which has to be considered when observing and modeling corresponding fluid transport processes.

3.2. Calculation of surface relaxation time distributions

To transform the measured NMR relaxation signals into their corresponding RTDs, a linear system of equations has to be solved. Because this inverse problem is generally ill-posed (Hadamard 1923), solving it is achieved by a regularized (smoothed) least square (LSQ) minimization (Aster *et al* 2005) of the form

$$\min \|\mathbf{Gm} - \mathbf{d}\|_2^2 + \lambda^2 \|\mathbf{Lm}\|_2^2 , \tag{5}$$

with $\mathbf{d} = E(t)$ the NMR data vector, $\mathbf{m} = I_i$ the model vector with relative intensities of the ith relaxation time bin and the forward operator $\mathbf{G}$ describing their physical relationship (see equations (1) and (2). $\mathbf{G}$ also accounts for both the bulk and, in case of T_2, the diffusion relaxation components that were determined in advance (see figure 3). The smoothness constraint on $\mathbf{m}$ is applied by a first-order derivative matrix $\mathbf{L}$. The regularization parameter λ is found via the L-curve criterion and chosen as such that the inversion misfit is in the order of the data noise while keeping a sufficiently smooth RTD (Hansen 1994, Aster *et al* 2005). All NMR data were processed, i.e. inverted using the open source software NUCLEUS (Hiller 2020).

It is important to note that the described algorithm computes the distributions of $T_{1S,i}$ and $T_{2S,i}$, i.e. the surface relaxation times, in contrast to the usual protocol of calculating $T_{1,i}$

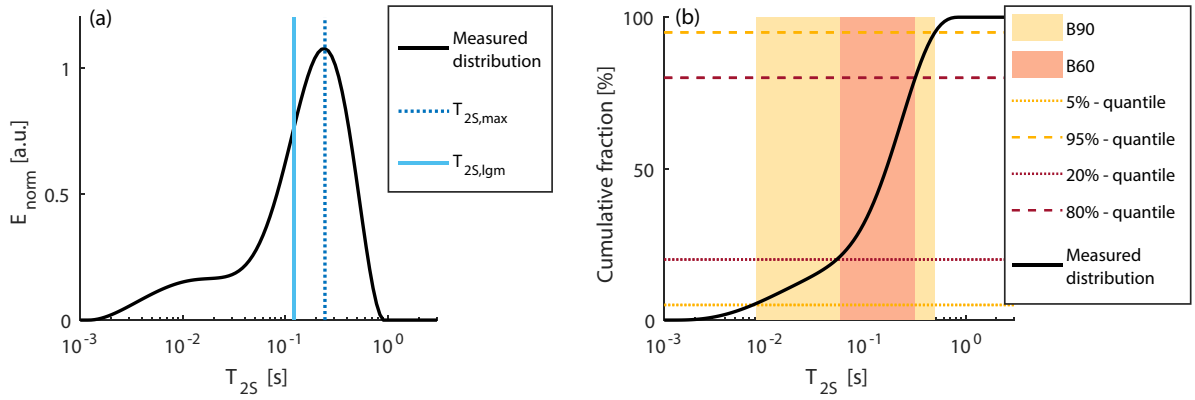

Figure 5. (a) distribution and (b) cumulative distribution of T_{2S} for the Berea sandstone sample and visualization of the characteristic quantities for the statistical analysis in this study: the T_{2S} time at the maximum ($T_{2S,max}$) and mean logarithmic of the distribution ($T_{2S,lgm}$), proportion between the 5% and 95% quantiles (B90), and between the 20% and 80% quantiles (B60). The same quantities were used to investigate the T_1 measurements.

and $T_{2,i}$ (see equations (1) and (2)). In other words, the effects of the bulk relaxation and in particular the diffusion relaxation (in case of measuring T_2 using SiS NMR) do not limit our resulting distributions. In doing so, we can directly compare the results of SiS and conventional NMR despite the bias that is expected for larger relaxation times (see figure 3) on the one hand. On the other hand, we focus the interpretation of our results on the substantial part of the relaxation mechanism that carries the pore size information.

We like to briefly put focus on the influence that the SNR of a particular NMR signal has on its corresponding RTD. As mentioned above, the applied LSQ inversion is constrained by a smoothness criterion ($\mathbf{L}$) and regularized in a manner to obtain the smoothest RTD within the noise of the NMR signal. Inevitably, this means that the larger the data noise is, the smoother, and hence also wider, the corresponding RTD will appear.

3.3. Relevant quantities characterizing the RTD

We analyze and compare the resulting RTDs by means of some characteristic quantities, e.g. the time of the RTD's global maximum $T_{2S,max}$ as a proxy of its main mode and its logarithmic mean $T_{2S,lgm}$ (figure 5(a)). The latter is commonly preferred for estimating permeability from NMR data using empirical models such as the Schlumberger-Doll Research equation (SDR, Kenyon (1997), Knight *et al* (2015)). Furthermore, we define two measures to characterize the broadness of the RTD (figure 5(b)): the differences of the T_2 times corresponding to the 20% and 80% quantiles (B60) of the cumulative RTD and those corresponding to the 5% and 95% quantiles (B90). The B60 criterion represents the main mode of the RTD associated with the most relevant range of pore sizes controlling the permeability characteristics. The B90 criterion also considers accompanying features at the RTD's periphery, e.g. additional smaller modes related to fractions of clay- or capillary bound water.

4. Results and discussion

4.1. Differentiation between T_2 and T_{2S} relaxation time distributions

As described above, when interpreting SiS NMR relaxation data it is necessary to consider the unavoidable diffusion relaxation rate due to the $\mathbf{B}_0$ gradient field that might cause a bias to the measured relaxation times. The practical consequence of this bias is demonstrated in figure 6, which compares different RTDs of the same saturated Berea sandstone sample. The RTD measured using conventional NMR for which the relation in equation (4) can be assumed, ranges from 0.001 s to 1 s. Almost 50% of it including its maximum at about 0.3 s exceed the SiS NMR threshold at $T_{2D} = 0.2$ s. Thus, the RTD measured by SiS NMR (orange-dotted) is compressed towards faster T_2 components <0.2 s. When taking the $1/T_{2D}$ term into account during the RTD calculation (orange), the information content in the range $>T_{2D}$ is reconstructed to some extent and matches the conventional RTD much better.

We use the RMS of the difference between the RTDs from conventional (as reference) and SiS NMR as quality criterion to demonstrate the effect of considering $1/T_{2D}$ for all of our samples. Figure 7 shows the corresponding overview, for which the samples are sorted with respect to their $T_{2S,lgm}$ in ascending order on the x-axis. Obviously, for 11 samples with higher $T_{2S,lgm}$ the consideration of $1/T_{2D}$ in the RTD calculation leads to an improved agreement with the reference measurement.

4.2. Comparison of T_{1S} and T_{2S} measurements using SiS and conventional NMR

In contrast to T_2 measurements, significant differences in the T_1 relaxation results of both NMR systems are not expected. However, we demonstrate and discuss the T_1 results by interpreting them as a benchmark of how good the agreement is under similar measurement conditions. At the top of figure 8,

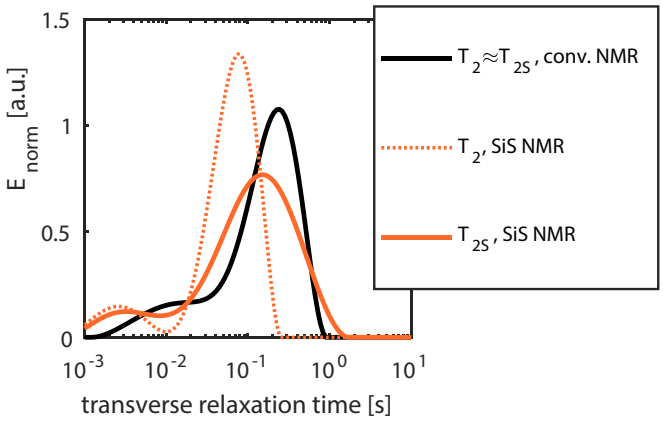

Figure 6. Relaxation time distributions (RTDs) of the Berea sandstone sample as measured with conventional and SiS NMR. The two SiS NMR curves demonstrate the necessity of taking the diffusion relaxation rate ($T_{2D} = 0.2$ s) into account for the RTD calculation.

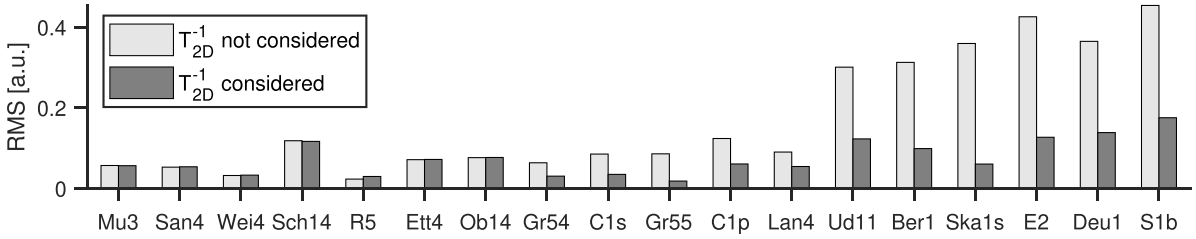

Figure 7. Root mean square (RMS) values of the difference between the relaxation time distributions measured by conventional and single-sided NMR with (dark gray columns) and without (light gray columns) consideration of the diffusion relaxation rate $1/T_{2D}$. The samples are sorted along the x-axis with respect to their $T_{2S,lgm}$ in ascending order.

the T_{1S} curves of three examplary sandstones are shown. The mean pore sizes of these examples increase from left to right. The measured SiS NMR relaxation curves as well as their RTDs (yellow) are in good agreement with the conventional ones (black). However, we note differences regarding some small details. The SiS NMR result (T_{1S}) of the sample Cs (figure 8(b)) exhibits a unimodal behavior with a broad maximum, which is in contrast to the slightly bimodal behavior of the reference measurement. The reason for this difference is the lower SNR of the SiS NMR measurement, which prohibits the correct reconstruction of the original bimodal shape. The slightly worse SNR of the SiS NMR data is also the reason for the overestimated broadness of the RTD of the sample Sb1 in figure 8(c). This effect was expected beforehand, as explained in section 3.2.

Figures 8(d)–(f) depict the T_{2S} data of the three examples. For the samples Wei and Cs (figures 8(d) and (e)), the main modes of the RTDs are in agreement. For these two samples, T_{2S} relaxation components below 0.05 s predominate due to their overall small pore sizes. In these cases, T_{2D} does not have an effect on the RTD (see figure 3). In contrast, we observe that those parts of the RTD >0.05 s are not correctly reconstructed by the SiS NMR measurement, because the influence of T_{2D} covers this information content in the measured signal. The same is true for the Sb1 sample depicted in figure 8(f). For this sample, however, the situation is much more crucial, because the main mode of its (conventional) RTD completely lies in the range higher than $T_{2S} = 0.2$ s. Hence, the SiS NMR result is not able to reconstruct the correct RTD. Instead, the main mode and the second mode at fast T_2 times between 0.01 and 0.1 s are merged to one broad monomodal distribution with an overall width even larger than the original one.

In the following, we perform a more generalized comparison of the two NMR techniques by evaluating the different RTD criteria as defined in section 3.3. We start with the T_1 measurements and the corresponding cross plots in figures 9(a)–(c). The linear regression coefficients (m_{lin}) and coefficients of determination (R^2) can be found in table 3. The attributes $T_{1S,max}$ (figure 9(a)) and B60 (figure 9(c)) are in almost perfect agreement, whereas $T_{1S,lgm}$ (figure 9(b)) tends to slight overestimation when measured with SiS NMR. This characteristics is directly linked to the trend of overestimating the B90 criterion and was already observed for the example in figure 8(c). Because the SiS NMR measurements exhibits a slightly higher SNR compared to the conventional measurements, the overall broadness of their RTDs and correspondingly their logarithmic mean is overestimated.

Figures 9(d)–(f) shows the cross plots for the T_2 criteria in the same manner as for T_1 in the top row. Please note the corresponding statistical quantities in table 3. Obviously, $T_{2S,max}$ and $T_{2S,lgm}$ measured by SiS NMR are systematically

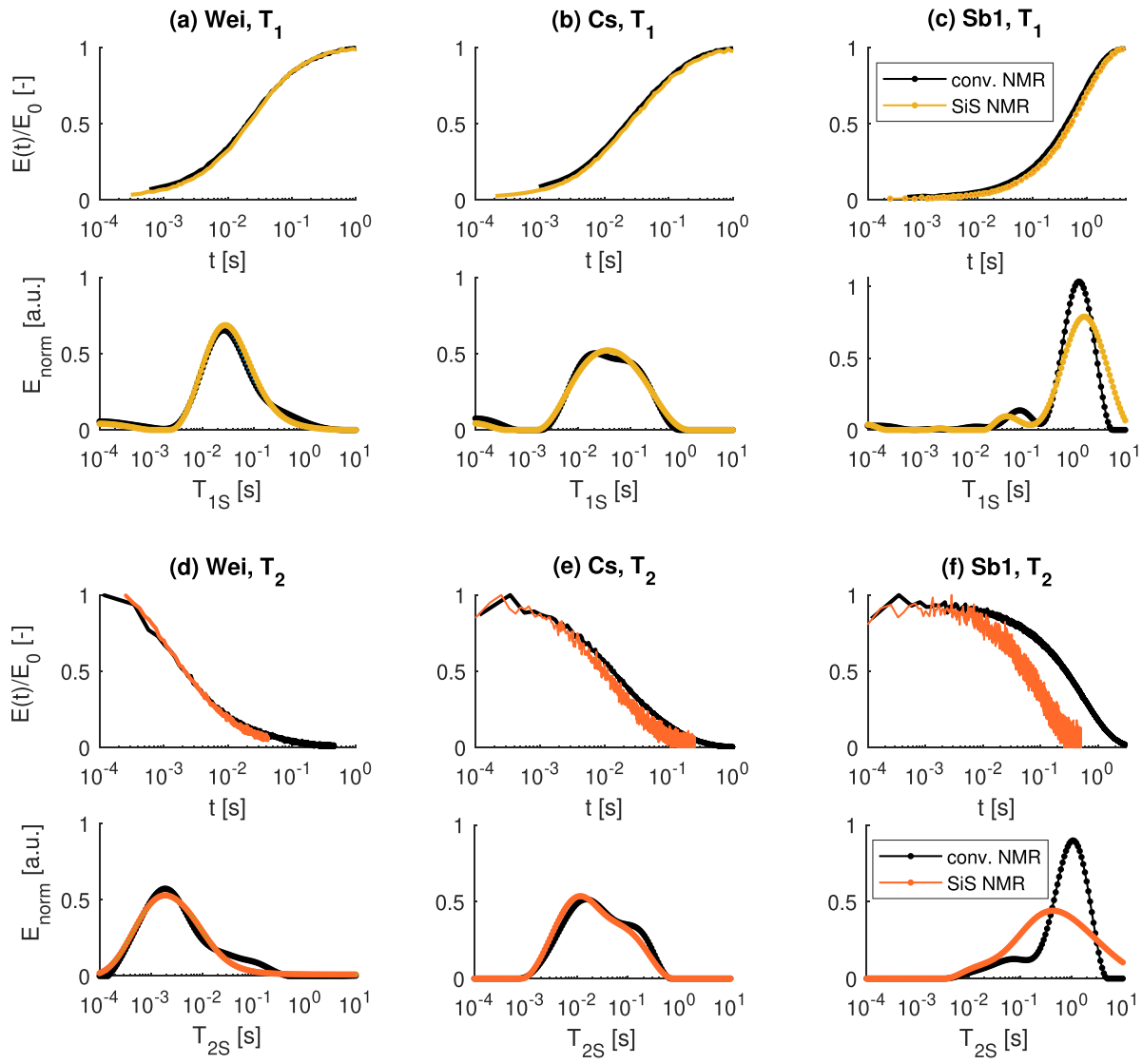

Figure 8. Data Examples for (a)–(c) longitudinal and (d)–(f) transverse relaxation curves as measured using single-sided (SiS) and conventional NMR and corresponding T_{1S} and T_{2S} time distributions for three sandstone samples: Wei (left), Cs (middle), and Sb1 (right).

underestimated. The corresponding regression coefficients demonstrate that these attributes are on average about 60% ($T_{2S,max}$) and 71% ($T_{2S,lgm}$) shorter than those measured conventionally. The RTD widths, as indicated by B60 and B90, are overestimated by the SiS data. This effect was expected beforehand and already shown and explained in figures 3 and 8: $T_{2S,max}$ times longer than $T_{2D} = 0.05$ s are attenuated and the attempt to reconstruct them blurs this weak information content over a range larger than the reference RTD.

4.3. Investigation of sub-millimeter bedding structure of a layered sandstone

Finally, we want to show and discuss the SiS NMR results on the vertical profile of the Berea sample as an example for a layered sandstone with obvious changes of lithology in the sub mm range. Figure 10 shows a photograph of the sample's front face overlaid by a diagram of the $T_{2S,lgm}$ times as a function of the measurement height. Obviously, the reddish layers are associated with reduced NMR relaxation times compared to the gray ones. Shorter relaxation times correspond to lower permeabilities, which is plausible for the Berea sandstone according to the study of Sato *et al* (2019). As they illuminate, the layers of Berea sandstone with accumulations of opaque minerals appear to be much less permeable to pore liquids than those without and report the ratio of the permeability measurements parallel and perpendicular to the bedding to be 8.5. They point out in their paper that determining the anisotropy characteristics of geological formations is desirable for a number of applications such as reservoir modeling, observation of contaminant waste disposal and CO_2 storage. However, the experimental effort to get this kind of data is great to date and could significantly be reduced using SiS NMR

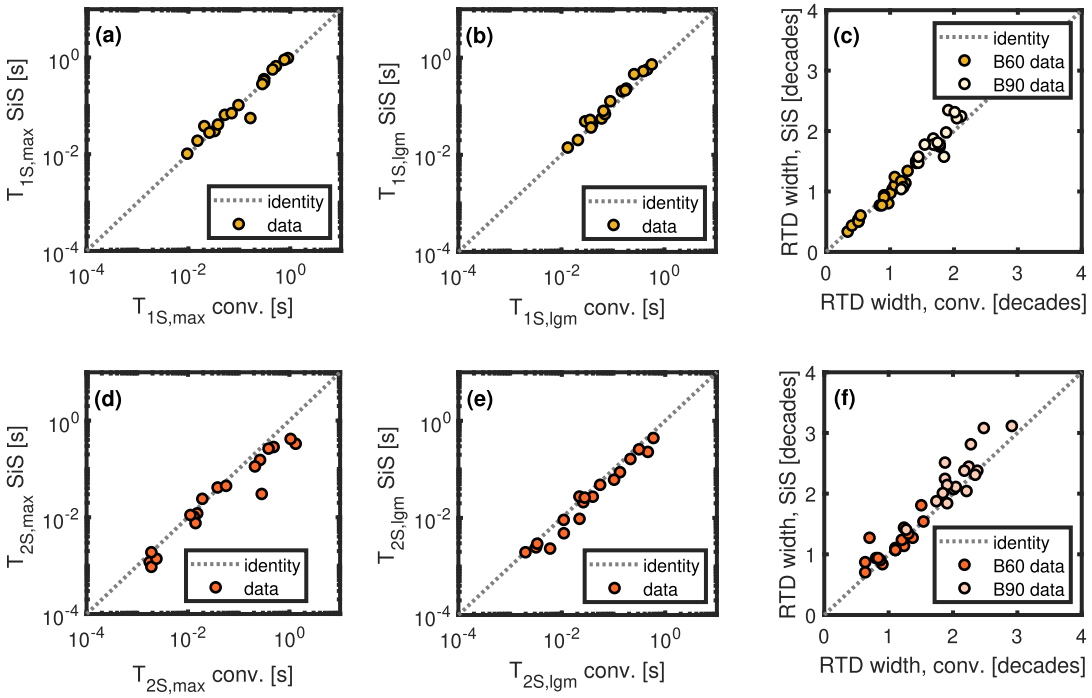

Figure 9. Cross plots comparing various statistical attributes characterizing the longitudinal (T_1) and transverse (T_2) relaxation time distributions (RTDs) as measured using single-sided (SiS) and conventional laboratory NMR (see also figure 5).

Table 3. List of statistic quantities for the T_1 and T_2 data in figure 9, respectively: the linear regression coefficient m_{lin} and the coefficient of determination corresponding to m_{lin} (R_m^2).

Quantity	$m_{\text{lin}}(T_1)$	R_m^2 (T_1)	$m_{\text{lin}}(T_2)$	R_m^2 (T_2)
$T_{1,2S,\text{max}}$	1.07	0.98	0.60	0.82
$T_{1,2S,\text{lgm}}$	1.24	0.96	0.71	0.95
B60	1.00	0.92	1.05	0.60
B90	1.06	0.81	1.09	0.72

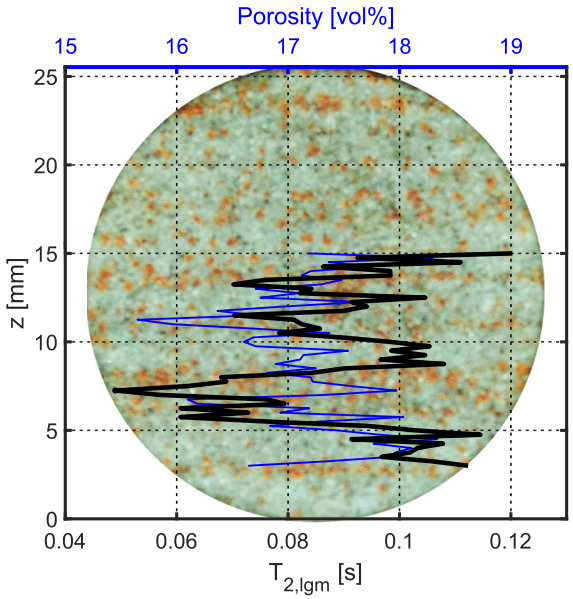

Figure 10. Mean logarithmic relaxation time and porosity as measured using SiS NMR as function of the height z of the sensitive measurement volume.

5. Summary

We identify two crucial issues regarding the application of SiS NMR compared to conventional geoscientific laboratory NMR technology that have a significant impact on the measurement performance. First, the additional diffusion relaxation rate $1/T_{2D}$ caused by the unavoidable gradient in $\mathbf{B}_0$: as we demonstrated, corresponding T_2 measurements are already biased at relaxation components much faster than 0.2 s (see figures 3 and 8), which is the limit given by T_{2D} for the used equipment in this study. Second, the SNR of SiS NMR measurements is generally lower due to the decreased sensitive volume compared to, for instance, NMR-based core scanners with a sensing volume of several cubic centimeters. This is true for both T_1 and T_2 and cannot be completely compensated by higher averaging (or stacking) rates. The corresponding increase in total measurement times would exceed an acceptable level, beyond which the application is no longer reasonable from a practical viewpoint. Regarding the SNR issue, our experimental setup might not be optimal, because we use cylindrical drill cores that fill less than half of the sensitive volume. However, in favor of a direct comparison with conventional NMR measurements using the very same samples, we accept this experimental shortcoming and compensate it to some extend by allowing SiS NMR measurement times much longer than those of the conventional NMR (see table 2).

Regarding T_1, our data demonstrates that SiS NMR provides results comparable to conventional NMR measurements. Caused by the lower SNR mentioned above, the widths of the RTDs measured by SiS NMR tend to overestimation. Moreover, small features at the periphery of the RTD and an equally weighted multimodal RTD shape might not be resolved properly (figure 8(b)). However, we do not expect a significant bias of hydraulic estimates from SiS NMR data, because $T_{1S,lgm}$ values and the principle range of relaxation times are captured correctly. Also regarding T_2, expedient SiS NMR measurements can be provided by SiS NMR despite the influence of T_{2D}. RTDs with main relaxation modes faster than 0.05 s are reconstructed correctly, whereas the attempt to reconstruct longer T_{2S} times blurs the information content over a range exceeding the correct RTD (see figure 8(f). However, for our samples including those with mean SiS NMR relaxation modes larger than $T_{2D} = 0.2$ s, the most important quantities $T_{2S,max}$ and $T_{2S,lgm}$ were found on average to be at only 60% and 71% of those from conventional NMR (table 2). We conclude that the corresponding permeability estimates if computed with, for instance, the SDR equation (Kenyon 1997) might still be reasonable despite this bias. Hydraulic parameters such as permeability are usually expected within a natural uncertainty of up to a magnitude.

6. Conclusion

Because of its mobility, SiS NMR enables new application fields in geosciences, as introduced above. In this study, we compare T_1 and T_2 data of diverse sandstones measured by SiS NMR with conventional NMR data. In general, the SNR of SiS NMR data must be expected to be lower than that of conventional laboratory devices, which might yield slightly overestimated RTD widths and consequently overestimated widths of the corresponding pore size distributions. This is generally true for both T_1 and T_2 data. However, for a potential usage in the identified application fields (a)–(d) in section 1, a corresponding cost-benefit-assessment has to be made, because in total longer averaging measurement times must be anticipated for SiS NMR measurements to achieve a comparable data quality.

In general, T_2 measurements are provided with much faster progress than T_1 and are thus preferred in practice. However, unbiased SiS NMR results for T_2 relaxation measurements can only be expected for fine materials, i.e. clayey or silty sediments and soils as well as sedimentary rocks with relaxation times smaller than about 0.05 s. For coarser materials, due to the T_{2D} relaxation in the external $\mathbf{B}_0$ gradient field, the resulting pore size distribution is not reconstructed correctly. Relaxation components above the T_{2D} limit are strongly attenuated, i.e. shifted towards smaller relaxation times. This distortion is corrected to some extent, if the diffusion relaxation is considered in the inversion process to produce the RTDs. However, such reconstruction leads to a certain bias towards large pore sizes and the trend to merge multimodal distributions into one broad mode. This is because the information content of the RTD above the T_{2D} limit is blurred over a large range by the smoothness constraints of the data inversion. However, for rough estimates of hydraulic parameters the SiS NMR method might still be feasible, because logarithmic mean and the general range of pore sizes are reconstructed within the correct magnitude. In any way, the total water content estimation remains undisturbed; T_{2S} relaxation components above the T_{2D} limit are not lost, only associated with incorrect relaxation regimes, i.e. they appear at a wrong position on the T_2 axis.

Regarding these findings, SiS NMR can potentially be helpful when identifying wet spots or leakage fissures on tunnel walls and can thus support activities to maintain safety and integrity of underground facilities. In particular it is very suitable for clay rock with T_{2S} times faster than 0.002 s, which is in the focus of current research as host rock for permanent repositories of radioactive waste material. SiS NMR is also a potential tool for soil moisture measurements and might provide calibration and control data for indirect remote methods. At least for fine soils, additional pore information can be expected from accompanying in-situ SiS NMR measurements.

The greatest opportunity provided by SiS NMR technology is the acquisition of profile relaxation data for rocks with significant bedding structures at the µm scale. Conventional magnetic resonance imaging techniques, although providing interesting images and even 3D data of porous systems, are not able to resolve stratification in the sub-millimeter range. With this feature, SiS NMR might be helpful for understanding and modeling electric, hydraulic, and diffusional anisotropy behavior of sedimentary rocks.

Data availability statement

The data that support the findings of this study are openly available at the following URL/DOI: 10.5281/zenodo.6511549.

Conflict of interest

The authors declare that they have no conflict of interest.

Ethics statement

The authors declare that this article does not contain any studies involving human or animal participants.

Funding statement

The authors received no particular financial support for the research work presented in this article.

ORCID iDs

Stephan Costabel https://orcid.org/0000-0003-3103-9760
Thomas Hiller https://orcid.org/0000-0002-5581-8673
Raphael Dlugosch https://orcid.org/0000-0001-6121-3120
Sabine Kruschwitz https://orcid.org/0000-0002-6296-4417
Mike Müller-Petke https://orcid.org/0000-0002-2001-9441

References

Anferova S, Anferov V, Arnold J, Talnishnikh E, Voda M A, Kupferschläger K, Blümler P, Clauser C and Blümich B 2007 Improved Halbach sensor for NMR scanning of drill cores *Magn. Reson. Imaging* **25** 474–80

Aster R C, Borchers B and Thurber C H 2005 *Parameter Estimation and Inverse Problems* (Amsterdam: Elsevier) (https://doi.org/10.1016/C2015-0-02458-3)

Behroozmand A, Keating K and Auken E 2014 A review of the principles and applications of the NMR technique for near-surface characterization *Surv. Geophys.* **36** 27–85

Blümich B, Perlo J and Casanova F 2008 Mobile single-sided NMR *Prog. Nucl. Magn. Reson. Spectrosc.* **52** 197–269

Carr H and Purcell E 1954 Effects of diffusion on free precession in nuclear magnetic resonance experiments *Phys. Rev.* **94** 630–8

Coates G R, Xiao L and Prammer M G 1999 *NMR Logging Principles and Application* (Huston: Halliburton Energy Services)

Costabel S, Hiller T and Kruschwitz S 2022 Nuclear magnetic resonance data of sandstones samples *dataset* (Zenodo) (https://doi.org/10.5281/zenodo.6511549)

Costabel S, Weidner C, Müller-Petke M and Houben G 2018 Hydraulic characterisation of iron-oxide-coated sand and gravel based on nuclear magnetic resonance relaxation mode analyses *Hydrol. Earth Syst. Sci.* **22** 1713–29

Dlugosch R, Günther T, Müller-Petke M and Yaramanci U 2013 Improved prediction of hydraulic conductivity for coarse-grained, unconsolidated material from nuclear magnetic resonance *Geophysics* **78** EN55–EN64

Dunn K J, Bergman D J and Latorraca G A 2002 *Nuclear Magnetic Resonance, Petrophysical and Logging Applications* 1st edn (Oxford: Pergamon)

Flaum C, Kleinberg R L and Bedford J 1998 Bound water volume, permeability and residual oil saturation from incomplete magnetic. Resonance logging data *SPWLA 39th Annual Logging Symp.* p 14

Hadamard J 1923 *Lectures on Cauchy's Problem in Linear Partial Differential Equations* (New York: Yale University Press)

Halbach K 1980 Design of permanent multipole magnets with oriented rare earth cobalt material *Nucl. Instrum. Methods* **169** 1–10

Hansen P 1994 Regularization tools: a matlab package for analysis and solution of discrete ill-posed problems *Numer. Algorithms* **6** 1–35

Hiller T 2020 ThoHiller/nmr-nucleus: v0.1.10 software (Zenodo) (https://doi.org/10.5281/zenodo.6984357)

Hiller T, Hoder G, Amann-Hildenbrand A, Klitzsch N and Schleifer N 2020 Two-phase fluid flow experiments monitored by NMR *E3S Web Conf.* **146** 03005

Keating K and Knight R 2007 A laboratory study to determine the effect of iron oxides on proton NMR measurements *Geophysics* **72** E27–E32

Keating K, Knight R and Tufano K J 2008 Nuclear magnetic resonance relaxation measurements as a means of monitoring iron mineralization processes *Geophys. Res. Lett.* **35** L19405

Kenyon W E 1997 Petrophysical Principles of Applications of NMR Logging *Log Anal.* **38** 21–43

Kleinberg R L and Horsfield M A 1990 Transverse relaxation processes in porous sedimentary rock *J. Magn. Reson. (1969)* **88** 9–19

Kleinberg R L, Sezginer A, Griffin D D and Fukuhara M 1992 Novel NMR apparatus for investigating an external sample *J. Magn. Reson. (1969)* **97** 466–85

Knight R, Walsh D O, Butler J J, Grunewald E, Liu G, Parsekian A D, Reboulet E C, Knobbe S and Barrows M 2015 NMR logging to estimate hydraulic conductivity in unconsolidated aquifers *Groundwater* **54** 104–14

Koch M, Schodlok M C, Guggenberger G and Stadler S 2021 Effects of water tension and surface roughness on soil hyperspectral reflectance *Geoderma* **385** 114888

Kolz J, Goga N, Casanova F, Mang T and Bluemich B 2007 Spatial Localization with Single-Sided NMR Sensors *Appl. Magn. Reson.* **32** 171–84

Lesparre N, Girard J-F, Jeannot B, Weill S, Dumont M, Boucher M, Viville D, Pierret M-C, Legchenko A and Delay F 2020 Magnetic resonance sounding measurements as posterior information to condition hydrological model parameters: application to a hard-rock headwater catchment *J. Hydrol.* **587** 124941

Levitt M H 2002 *Spin Dynamics - Basics of Nuclear Magnetic Resonance* (New York: Wiley)

Meiboom S and Gill D 1958 Modified Spin-echo Method for Measuring Nuclear Relaxation Times *Rev. Sci. Instrum.* **29** 688–91

Müller-Petke M, Dlugosch R, Lehmann-Horn J and Ronczka M 2015 Nuclear magnetic resonance average pore-size estimations outside the fast-diffusion regime *Geophysics* **80** D195–206

Müller-Petke M and Yaramanci U 2015 Tools and techniques: nuclear magnetic resonance *Treatise on Geophysics* 2nd edn, vol 11 ed G Schubert (Oxford: Elsevier) pp 419–45

Pape H, Tillich J E and Holz M 2006 Pore geometry of sandstone derived from pulsed field gradient NMR *J. Appl. Geophys.* **58** 232–52

Perlo J, Casanova F and Blümich B 2005 Profiles with microscopic resolution by single-sided NMR *J. Magn. Reson.* **176** 64–70

Romanenko K, Xiao D and Balcom B J 2012 Velocity field measurements in sedimentary rock cores by magnetization prepared 3d sprite *J. Magn. Reson.* **223** 120–8

Sato M, Panaghi K, Takada N and Takeda M 2019 Effect of bedding planes on the permeability and diffusivity anisotropies of Berea sandstone *Transp. Porous Media* **127** 587–603

Schulte Holthausen R and Raupach M 2018 Monitoring the internal swelling in cementitious mortars with single-sided 1h nuclear magnetic resonance *Cement Concr. Res.* **111** 138–46

Seland J G, Washburn K E, Anthonsen H W and Krane J 2004 Correlations between diffusion, internal magnetic field gradients and transverse relaxation in porous systems containing oil and water *Phys. Rev.* E **70** 051305

Vouillamoz J M, Hoareau J, Grammare M, Caron D, Nandagiri L and Legchenko A 2012 Quantifying aquifer properties and freshwater resource in coastal barriers: a hydrogeophysical approach applied at Sasihithlu (Karnataka state, India) *Hydrol. Earth Syst. Sci.* **16** 4387–400

Walsh D *et al* 2013 A Small-Diameter NMR Logging Tool for Groundwater Investigations *Groundwater* **51** 914–26

Zhang Z and Weller A 2014 Fractal dimension of pore-space geometry of an eocene sandstone formation *Geophysics* **79** D377–87

Ziefle G, Matray J-M, Maßmann J and Möri A 2017 Coupled hydraulic-mechanical simulation of seasonally induced processes in the mont terri rock laboratory (switzerland) *Swiss J. Geosci.* **110** 195–212